



The study of radical cations of $\text{Me}_3\text{C-SiMe}_3$ and $\text{Me}_3\text{C-GeMe}_3$ in alkane solutions using the method of time-resolved magnetic field effect and DFT calculations

V.I. Borovkov^{a,b}, P.A. Potashov^b, V.A. Bagryansky^a, Yu.N. Molin^a, V.I. Faustov^{c,*},
I.V. Krylova^c, M.P. Egorov^c

^aInstitute of Chemical Kinetics and Combustion, Siberian Branch of the Russian Academy of Sciences, Institutskaya Street 3, 630090 Novosibirsk, Russian Federation

^bNovosibirsk State University, Pirogova Street, 2, 630090 Novosibirsk, Russian Federation

^cN.D. Zelinsky Institute of Organic Chemistry, Russian Academy of Sciences, Leninsky Prosp. 47, 119991 Moscow, Russian Federation

ARTICLE INFO

Article history:

Received 25 June 2008

In final form 7 October 2008

Available online 11 October 2008

ABSTRACT

Radical cations of $\text{Me}_3\text{CSiMe}_3$ and $\text{Me}_3\text{CGeMe}_3$ were detected in hexane solution using the method of time-resolved magnetic field effect. The structures and electronic distributions of neutral molecules Me_3CEMe_3 and their radical cations: $\text{Me}_3\text{CEMe}_3^+$ ($E = \text{C, Si, Ge, Sn}$) were investigated by DFT PBE/TZ2P calculations. The calculated and the experimental hyperfine coupling constants $a(\text{H})$ are in good agreement. The structures of $\text{Me}_3\text{CSiMe}_3^+$, $\text{Me}_3\text{CGeMe}_3^+$, and $\text{Me}_3\text{CSnMe}_3^+$ are in essence a tight radical cation pairs of the type $\text{CMe}_3/\text{EMe}_3^+$.

© 2008 Published by Elsevier B.V.

1. Introduction

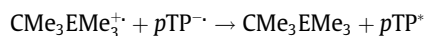
It is known that oxidizing of Group 14 element organometallic compounds to radical cations (RC) easily took place due to their comparatively low ionization potentials [1]. Detection and quantum chemical study of these transient species is of fundamental importance from the point of view of establishing their structure and reaction mechanisms. Recently, to study RC of Group 14 element organometallics EMe_4 and symmetric Me_3EEMe_3 ($E = \text{Si, Ge, Sn}$) in irradiated liquid solution, the method of time-resolved magnetic field effect (TR MFE) was applied successfully [2]. The spin evolution of spin correlated radical ion pairs involving the RC under study was monitored by time resolved fluorescence arising upon recombination of the pairs. This approach allowed for determining of g -factors and isotropic hyperfine coupling (HFC) constants for those RCs as well as estimating their lifetimes in liquid solution.

This Letter reports the detection of RCs of nonsymmetrical $\text{Me}_3\text{CSiMe}_3$ and $\text{Me}_3\text{CGeMe}_3$ compounds in liquid hexane. To get more insight into structure of these species we carried out quantum chemical DFT PBE calculations on Me_3CEMe_3 ($E = \text{C}$ (1), Si (2), Ge (3), Sn (4)) and their radical cations $\text{Me}_3\text{CEMe}_3^+$, ($1^+ - 4^+$) as well as some of their fragments: radicals EMe_3 and cations EMe_3^+ .

2. Experimental and computational details

2.1. Method

RCs of studied organometallics were generated by irradiation of n -hexane solutions of the compounds with 2-ns pulses of X-rays with quantum energy of about 20 keV using a nanosecond X-ray fluorimeter described elsewhere [3]. The radiation-initiated fluorescence of the solutions, which also included the 30 μM of *para*-terphenyl- d_{14} (*pTP*) as an electron acceptor and luminophor, was detected by single photon counting method. The light was collected using an optical bandpass filter (260–390 nm) to select the fluorescence of *pTP*^{*}, which appears via radical ions recombination



To measure the influence of an external magnetic field on the fluorescence, the sample cuvette constructed without using ferromagnetic materials was situated between magnet poles with magnetic field induction up to 1.1 T. The fluorescence was registered in zero and strong magnetic fields, alternatively, for periods of 250 s. Zero magnetic field was adjusted to within ± 0.05 mT. The solutions were degassed by repeated freeze-pump-thaw cycles. All measurements were made at 293 ± 0.5 K.

2.2. Materials

n -Hexane used as a solvent was stirred with concentrated sulfuric acid, washed with water, distilled over sodium and passed through a 1 m column of activated alumina. *para*-Terphenyl- d_{14}

* Corresponding author. Fax: +7 499 1358941.

E-mail addresses: borovkov@kinetics.nsc.ru (V.I. Borovkov), fau@ioc.ac.ru, fau-vi@yandex.ru (V.I. Faustov).

(98%) was received from Aldrich and used without additional purification.

tert-Butyltrimethylsilane was prepared by the reaction of commercially available *tert*-butyldimethylchlorosilane with methylmagnesiumbromide in 60% yield. *tert*-Butyltrimethylgermane was prepared by the reaction of chlorotrimethylgermane with *tert*-butyl lithium in 54% yield as described in Ref. [4].

2.3. Calculations

Quantum chemical calculations with full geometry optimization were carried out with the PBE density functional [5] using the PRIRODA program [6,7]. The three-exponent basis set TZ2P included two sets of polarization functions, namely, (5s2p) [3s2p] for H atoms, (11s6p2d) [6s3p2d] for C atoms, (15s11p2d) [10s6p2d] for Si atoms and (18s14p9d) [13s10p5d] for Ge atoms (figures in parentheses and in square brackets denote the initial and contracted basis set, respectively) and the electron density expansion over an auxiliary uncontracted basis set [7]: (5s2p) for H atoms, (10s3p3d1f) for C atoms, (14s3p3d1f1g) for Si atoms and (18s3p3d1f1g) for Ge atoms. Stationary points were characterized and confirmed by calculating and diagonalising the matrix of energy second derivatives. The final energies included the zero-point energy corrections, ZPE. The thermodynamic functions were calculated using the ‘harmonic oscillator–rigid rotator’ model.

2.4. Spin dynamics calculations

In this work the well-elaborated approach [8] to the calculations of dynamics of spin evolution of spin-correlated radical ion pairs (RIPs) was applied. According to that the ratio (MFE) of the delayed fluorescence decays as recorded at ($I_B(t)$) and without ($I_0(t)$) external magnetic field B may be represented as follows:

$$\frac{I_B(t)}{I_0(t)} \approx \frac{\theta \rho_{ss}^B(t) + \frac{1}{4}(1-\theta)}{\theta \rho_{ss}^0(t) + \frac{1}{4}(1-\theta)} \quad (1)$$

Here $\rho_{ss}(t)$ is the singlet spin population of initially singlet-correlated RIPs. θ is the empirical parameter, which allows one to take into account that the fraction of such RIPs differs from unity due to cross recombination in the radiation track. Indices B and 0 correspond to measurements at strong and zero magnetic field, respectively.

To describe the evolution of RIP’s spin state at high and zero fields expressions [8]

$$\rho_{ss}^B(t) = \frac{1}{4} + \frac{1}{4}e^{-\frac{t}{T_1}} + \frac{1}{2}e^{-\frac{t}{T_2}} \cos\left(\frac{\Delta g \beta B}{\hbar}\right) G_c^B(t) G_a^B(t) \quad (2)$$

$$\rho_{ss}^0(t) = \frac{1}{4} + \frac{3}{4}e^{-\frac{t}{T_0}} G_c^0(t) G_a^0(t) \quad (3)$$

were used. Here $1/T_1$ and $1/T_2$ are the rates of spin-lattice and phase relaxations, respectively. T_0 is the parameter introduced to account for paramagnetic relaxation in zero magnetic field. Δg is the difference between the g -values of RIP partners. $G(t)$ is the function as determined by HFC constants in corresponding radical ion only. Indices ‘c’ and ‘a’ in Eqs. (2) and (3) indicate the radical cation and radical anion, respectively.

Calculation of $G_a(t)$, that is the contribution of $pTP^{\cdot-}$ to spin dynamics, was performed using semiclassical approximation [9]. According to that

$$G_a^0(t) = \frac{1}{3} \left[1 + 2(1 - \gamma^2 \sigma^2 t^2) \cdot e^{-\frac{\gamma^2 \sigma^2 t^2}{2}} \right] \quad (4)$$

$$G_a^B(t) = e^{-\frac{\gamma^2 \sigma^2 t^2}{2}} \quad (5)$$

Here σ^2 is the second moment of ESR spectrum of radical anion, γ is the gyromagnetic ratio for electron.

To evaluate $G_c(t)$ for RCs $2^{\cdot+}$ or $3^{\cdot+}$, which did contain two groups of magnetically equivalent nuclei, recently developed theoretical approach was applied [10]. The particular expressions are rather complex and may be found in the original paper. To provide more reliable comparison between the experimental and calculated TR MFE curves the temporal dependencies of $\rho_{ss}(t)$ in Eq. (1) were convoluted with functions $h(t) = \exp(-t^2/\omega^2)/(\pi\omega)^{1/2}$ ($\omega = 2$ ns) and $f(t) = \exp(-t/\tau)/\tau$ ($\tau = 1$ ns). The $h(t)$ function allows us to take into account a particular time-response function of the experimental equipment while the $f(t)$ is introduced to account for luminophore fluorescence lifetime [10].

3. Results and discussion

3.1. Experimental results

In Figs. 1 and 2 are shown experimental and calculated TR MFE curves for $2^{\cdot+}$ and $3^{\cdot+}$, obtained for *n*-hexane solutions of 0.1 M of **2** (Fig. 1) and **3** (Fig. 2) at $B = 0.1$ T and 1.1 T. In these figures the TR MFE curves for $1^{\cdot+}$ obtained for 0.1 M solutions of **1** at $B = 0.1$ T are presented also by dashed line. Note that TR MFE curves obtained

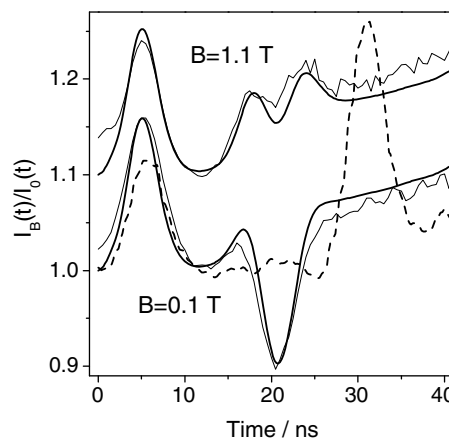


Fig. 1. The experimental and the calculated (smooth lines) TR MFE curves as obtained for irradiated solution of 0.1 M *tert*-butyltrimethylsilane **2** in *n*-hexane (+30 μ M pTP) at $B = 0.1$ T and 1.1 T. The modeling parameters are given in Table 1. By dashed line the experimental curve for 0.1 M hexamethylethane **1** solution in *n*-hexane (+30 μ M pTP) is shown [11].

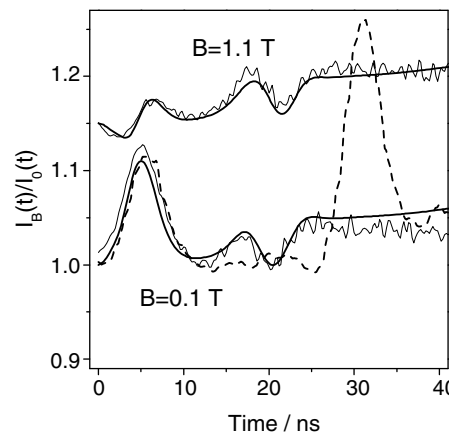


Fig. 2. The experimental and the calculated (smooth lines) TR MFE curves as obtained for irradiated solution of 0.1 M *tert*-butyltrimethylgermane **3** in *n*-hexane (+30 μ M pTP) at $B = 0.1$ T and 1.1 T. The modeling parameters are given in Table 1. By dashed line the experimental curve for 0.1 M hexamethylethane **1** solution in *n*-hexane (+30 μ M pTP) is shown [11].

for 1^+ were analyzed in detail earlier [11]. Unpaired electron in 1^+ couples with 18 β -protons whose equivalence is provided by fast rotations of methyl groups and, very probable, of *tert*-butyl fragment around elongated central C–C bond.

Let us first discuss the results obtained at $B = 0.1$ T. All the TR MFE curves presented display several distinctive peaks. Importantly, weak HFC in radical anion pTP^- is not capable to contribute significantly to this pattern within the time range under study and the spin evolution is to be determined by HFCs in corresponding RCs.

The first peak in TR MFE curves (<10 ns) is determined by the second moment of ESR spectrum of RCs [8]. The minor difference between the peaks for the solutions **1**, **2**, and **3** indicates similar values of the second moment of ESR spectrum, σ^2 , for radical cations in all the cases.

The next peaks are at about 20 ns in TR MFE curves for 2^+ and 3^+ and these are opposite in their relative sign as compared to the second peak observed for 1^+ at approximately 30 ns. It was shown earlier [12] that in the case of RC, having HFC with magnetically equivalent nuclei only, the time positions of the second peak is determined by HFC constant value with the time shift being larger for smaller constants. Besides, such a peak is positive if the number of the equivalent nuclei is even while this becomes negative when the number is odd.

Thus, the sign and time positions of the second peaks on the TR MFE curves for 2^+ and 3^+ indicate unambiguously that in these RCs

- 1) unpaired electron interacts, mainly, with odd magnetically equivalent protons;
- 2) the dominant HFC constants are larger than those of 1^+ .

As will be shown below these conclusions are in excellent agreement with results of our quantum chemical calculations.

Then, increasing magnetic field induction affects noticeably the TR MFE curves. It suggests the significant difference between the g -values of organometallic RCs and those of pTP^- ($g \approx 2.0027$ [13]). The fit of the experimental TR MFE curves obtained at different values of magnetic induction B allows one to estimate both the g -values and HFC constants in the radical cations. As follows from Figs. 1 and 2, the model of spin dynamics in spin-correlated RIPs used here works fairly good. It is significant that except the large HFC

constant a smaller one with 9 equiv. protons should be taken into account to properly simulate the curves. The parameter values providing the best fit for 2^+ and 3^+ are shown in Table 1.

The HFC values obtained are discussed in detail below. As for paramagnetic relaxation for 2^+ and 3^+ , it should be noted that the relaxation is rather fast except for spin-lattice relaxation of 2^+ , for which T_1 value has been estimated by the order of magnitude only. These relaxation parameters do not exhibit any significant field induction or concentration (up to 0.1 M) dependences that indicate negligible contribution of the degenerate electron transfer to the relaxation.

3.2. Calculation results

In contrast to ethane which ionization is known to produce several close in energy isomeric lower symmetry forms of $H_3CCH_3^+$ [14], in the case of its hexamethylated analog 1^+ we found only one minimum in which carbon skeleton has D_{3d} symmetry, i.e. the same as in neutral Me_3CCMe_3 . The C_{3v} symmetry of 2^+ – 4^+ skeletons is the same as that of neutral **2**–**4** molecules.

In neutral species **1**–**4** the length of central C–E bond has an expected order: $C \ll Si < Ge < Sn$ (Table 2). Ionization results in significant elongation of these bonds. The most dramatic effect is observed in 1^+ , where the calculated length of central C–C bond (2.685 Å) is longer than in any of $H_3CCH_3^+$ isomers (1.973 Å) [14], and even longer than the C–E bonds in hetero analogs 2^+ – 4^+ (Table 2).

In contrast to the central bond, other skeletal bonds (C–CH₃ or E–CH₃) are slightly contracted (by ca 0.04 Å) upon ionization. It is worth to note that configuration of CMe_3 and EMe_3 groups in **1**–**4** became less pyramidal in RCs 1^+ – 4^+ . This flattening becomes evident if we compare the sum of three valence angles of CMe_3 fragments in **1** (322.7) and 1^+ (354.5) with that of pure tetrahedral (328.8) and planar (360.0) configurations. Strong elongation of the central bond in 1^+ – 4^+ indicates its weakening and even possibility dissociation into CMe_3 and EMe_3 fragments with one bearing positive charge, other being neutral radical. To get insight into stability of radical ions we compared energies of homolytic cleavage of C–E bond in neutrals (1) and those of two pathways (2) and (3) of dissociation of charged species 1^+ – 4^+ (see Scheme 1).

The energies presented in Table 3 show that ionization of **1**–**4** brings dramatic fall of the strength of central C–E bonds which agrees with the observed changes in geometry discussed above. With $E = Si, Ge, Sn$ dissociation (2) to $EMe_3^+ + CMe_3$ is clearly favored over an alternative (3) $EMe_3 + CMe_3^+$. An analysis of electronic structures of neutral and ionized species shows this favorable dissociation pattern could be traced in 2^+ – 4^+ (Table 4).

Calculated and experimental hydrogen hyperfine coupling constants a_H in 1^+ – 4^+ and in some radicals, which could be produced in reactions (1)–(3) are collected in Table 4. Calculated a_H values are averages over 9 protons of EMe_3 fragments. In the case of 1^+ we have two CMe_3 fragments which have identical a_H values.

Calculated a_H are in good agreement with the experimental values. The a_H value in 1^+ is about a half of a_H in CMe_3 . This suggests that distribution of spin density between C and H atoms in CMe_3 fragments of radical 1^+ follows the same pattern as in radical

Table 1

HFC constants, the g -values, and paramagnetic relaxation times as used for modeling of TR MFE curves shown in Figs. 1 and 2.

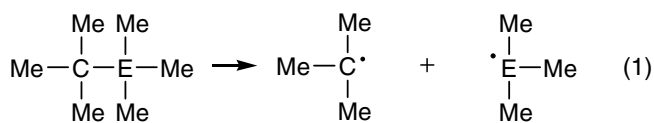
Radical cation	Parameters
Hexamethylethane ⁺ (1^+)	$a(18H) = 1.22$ mT; $g = 2.0034^a$
<i>tert</i> -Butyltrimethylsilane ⁺ (2^+)	$a(9H) = 1.87$ mT; $a(9H) = 0.26$ mT $g = 2.0044$ $T_2 = T_0 = 65$ ns; $T_1 = 1500$ ns
<i>tert</i> -Butyltrimethylgermane ⁺ (3^+)	$a(9H) = 1.87$ mT; $a(9H) = 0.3$ mT $g = 2.0116$ $T_2 = T_0 = 35$ ns; $T_1 = 100$ ns

^a Ref. [11].

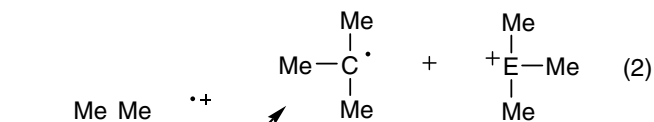
Table 2

The length of the central C(1)–E bond/Å, the valence angles C(1)–E–C and E–C(1)–C in EMe_3 – CMe_3 ($E = C, Si, Ge, Sn$) and their radical cations calculated with the PBE/TZ2P method.

E	Me_3CMe_3 C(1)–E	Me_3CMe_3 C(1)–E–C	Me_3CMe_3 E–C(1)–C	$Me_3CMe_3^+$ C(1)–E	$Me_3CMe_3^+$ C(1)–E–C	$Me_3CMe_3^+$ E–C(1)–C
C	1.590	111.3	111.3	2.685	97.9	97.9
Si	1.936	110.5	109.9	2.335	103.4	101.3
Ge	2.019	110.3	109.3	2.449	100.6	102.2
Sn	2.233	109.8	109.2	2.608	97.6	100.4



1 - 4

1⁺ - 4⁺

(E=C, Si, Ge, Sn)

Scheme 1.

Table 3
DFT PBE calculated total ΔE_0 ^a and Gibbs ΔG ^b energies/kcal mol⁻¹ for reactions (1)–(3).

	ΔE_0 for reaction			ΔG for reaction		
	(1)	(2)	(3)	(1)	(2)	(3)
CMe ₃ –CMe ₃	60.1	22.5	22.5	44.9	10.1	10.1
CMe ₃ –SiMe ₃	68.3	29.5	38.9	60.0	15.8	25.9
CMe ₃ –GeMe ₃	60.6	27.4	36.3	54.3	15.1	23.3
CMe ₃ –SnMe ₃	51.0	26.8	34.5	46.9	16.8	21.7

^a $\Delta E_0 = \Delta E + \text{ZPE}$.^b At $T = 298 \text{ K}$ and $p = 1 \text{ atm}$.

Table 4
DFT PBE calculated and experimental hyperfine coupling constants a_{H} (H)/mT.

Radical	Fragment	a_{H} calc	a_{H} exp	Ref.
1 ⁺	Me ₃ CCMe ₃	1.17	1.22	[11]
2 ⁺	[CMe ₃]	1.82	1.87	This work
2 ⁺	[SiMe ₃]	0.27	0.26	This work
3 ⁺	[CMe ₃]	1.82	1.87	This work
3 ⁺	[GeMe ₃]	0.27	0.3	This work
4 ⁺	[CMe ₃]	1.92	–	–
4 ⁺	[SnMe ₃]	0.16	–	–
•CMe ₃	CMe ₃	2.07	2.27	[15]
•SiMe ₃	SiMe ₃	0.62	0.63	[16]
•GeMe ₃	GeMe ₃	0.52	0.49	[16]
•SnMe ₃	SnMe ₃	0.32	0.28	[16]

Table 5
DFT PBE calculated fragment partitions of the charge and spin densities in 1⁺–4⁺/a.u.

Radical cation	Fragment	Charge	Spin
1 ⁺	[CMe ₃]	0.500	0.500
2 ⁺	[CMe ₃]	0.439	0.679
2 ⁺	[SiMe ₃]	0.562	0.322
3 ⁺	[CMe ₃]	0.417	0.675
3 ⁺	[GeMe ₃]	0.585	0.325
4 ⁺	[CMe ₃]	0.390	0.709
4 ⁺	[SnMe ₃]	0.611	0.291

•CMe₃. The situation is more complicated in hetero analogs 2⁺–4⁺. The simulation of TR MFE spectra of 2⁺ and 3⁺ gave two values of a_{H} for each species. The higher values of a_{H} for 2⁺ and 3⁺ are close to each other and according to our calculation should be assigned to CMe₃ fragments. About two thirds (67–71%) of unpaired spin density (Table 5) in 2⁺–4⁺ are located on CMe₃ fragment, the remaining third is on EMe₃. Total electronic density distributions on CMe₃ and EMe₃ fragments in 2⁺–4⁺ (Table 5) looks less polarized with relatively small (0.12–0.22 a.u.) excess of positive charge on EMe₃ fragment. These arguments suggest that the electronic structure of 2⁺–4⁺ could be seen as CMe₃/EMe₃⁺, and thus readily explains why their dissociation to EMe₃⁺ and CMe₃[•] fragments is energetically favored over an alternative route Me₃ + CMe₃[•].

4. Conclusions

By applying the method of time-resolved magnetic field effect the radical cations of Me₃CSiMe₃ and Me₃CGeMe₃ were observed in liquid hexane at room temperature for the first time and their HFC constants as well as g -values were determined. The RCs' identity was confirmed by the quantum chemical calculation of HFC constants in these radicals using DFT approach. No evidence for the RCs decay within time domain 0–100 ns was observed. At the same time, the unpaired electron spin density distribution in these RCs resembles species, which is partially dissociated into *tert*-butyl radical and cation of trimethylsubstituted Group 14 element organometallics.

Acknowledgements

The authors express their gratitude to Dr. D.N. Laikov for providing access to his program PRIRODA and to Profs. O.M. Nefedov and V.A. Radzig for valuable discussions. This work was financially supported by the RFBR (grants Nos 06-03-33010 and 07-03-00693), Presidential program for support of leading Research schools (grants Nos NSH-6075.2006.03 and Grant NSH-1875.2008.3), and the Russian Academy of Sciences (Programs P-09 and OX-01).

References

- [1] J. Iley, in: S. Patai (Ed.), *The Chemistry of Organic Germanium, Tin and Lead Compounds*, John Wiley & Sons Ltd., New York, 1995, p. 267.
- [2] V.I. Borovkov, V.A. Bagryansky, Yu.N. Molin, M.P. Egorov, O.M. Nefedov, *Phys. Chem. Chem. Phys.* 5 (2003) 2027.
- [3] S.V. Anishchik, V.M. Grigoryants, I.V. Shebolaev, Y.D. Chernousov, O.A. Anisimov, Yu.N. Molin, *Instrum. Exp. Tech.* 32 (4) (1989) 813, part 1.
- [4] C.F.I. Shaw, A.L. Allred, *J. Organomet. Chem.* 28 (1971) 53.
- [5] J.P. Perdew, K. Burke, M. Ernzerhof, *Phys. Rev. Lett.* 77 (1996) 3865.
- [6] D.N. Laikov, Y.A. Ustynyuk, *Russ. Chem. Bull.* 54 (2005) 820.
- [7] D.N. Laikov, *Chem. Phys. Lett.* 281 (1997) 151.
- [8] V.A. Bagryansky, V.I. Borovkov, Yu.N. Molin, *Russ. Chem. Rev.* 76 (2007) 493.
- [9] K. Schulten, P.G. Wolynes, *J. Chem. Phys.* 68 (1978) 3292.
- [10] V.A. Bagryansky, K.L. Ivanov, V.I. Borovkov, N.N. Lukzen, Yu.N. Molin, *J. Chem. Phys.* 122 (2005) 224503.
- [11] V.A. Bagryansky, V.I. Borovkov, Yu.N. Molin, *Phys. Chem. Chem. Phys.* 6 (2004) 924.
- [12] V.A. Bagryansky, O.M. Usov, V.I. Borovkov, T.V. Kobzeva, Yu.N. Molin, *Chem. Phys.* 255 (2000) 237.
- [13] M.T. Jones, in: H. Fischer, K.-H. Hellwege (Eds.), *V 9d1 Organic Anion Radicals*, Springer-Verlag, Berlin, Heidelberg, New York, 1980, p. 707.
- [14] H. Zuilhof, J.P. Dinnocenzo, C. Reddy, S. Shaik, *J. Phys. Chem.* 100 (1996) 15774.
- [15] F.A. Neugebauer, in: H. Fischer (Ed.), *V 17b Nonconjugated Carbon Radicals*, Springer-Verlag, Berlin, Heidelberg, New York, 1987, p. 5.
- [16] M. Lehnig, in: H. Fischer, K.-H. Hellwege (Eds.), *V 9c2 Organic O-, P-, S-, Se-, Si-, Ge-, Sn-, Pb-, As-, Sb-Centered Radicals*, Springer-Verlag, Berlin, Heidelberg, New York, 1979, p. 307.